



In Vitro Evaluation of Biologically Derived Hydroxyapatite Coatings Manufactured by High Velocity Suspension Spraying

M. Blum¹ · M. Sayed² · E. M. Mahmoud² · A. Killinger¹ · R. Gadow¹ · S. M. Naga²

Submitted: 25 May 2021 / in revised form: 21 September 2021 / Accepted: 28 September 2021 / Published online: 17 October 2021
© The Author(s) 2021

Abstract This investigation aims to study a novel biologically derived coating applied on Ti alloy substrates. Obtained from a low-cost fish bone resource, a nanocrystalline hydroxyapatite has been synthesized and converted to an organic suspension. Coating was then manufactured by a high-velocity suspension flame spray process. The microstructure, phase composition, coating thickness, and roughness of hydroxyapatite (HA)-coated samples were studied. The results indicated the presence of both hydroxyapatite and β -tricalcium phosphate phases and the final coating layer was uniform and dense. In vitro bioactivity and biodegradability of the HA/Ti composite samples were estimated by immersion in simulated body fluid. Remarkable reductions in Ca^{2+} and PO_4^{3-} ion concentrations were observed as well as low weight loss percentage and a slight variation in the pH value, indicating the generation of an apatite layer on the surface of all studied samples. Scanning electron microscopy, energy-dispersive x-ray analysis, and inductively coupled plasma–optical emission spectrometry confirm these results. Thus biological derived HA coatings are a promising candidate to enhance bioactivity and biodegradability of bone implants. To demonstrate feasibility on commercial medical components, a medical screw was coated and evaluated.

Keywords bioactive ceramic coatings · biodegradability · HVFS · hydroxyapatite (HA) · in vitro · thermal spraying

Introduction

Since the nineteenth century, metals have been used as implants for bone replacement. For metals to serve as replacement for load-bearing bones, they should have excellent mechanical properties and a bioinert reaction toward human body tissues. Although many metals have good mechanical characteristics, only a few of them are biocompatible. Cobalt-, stainless-steel-, and titanium-based alloys are biocompatible metals widely used as implant materials (Ref 1). In comparison with other metallic implants, titanium alloys are extensively utilized for implantation due to their favorable properties. Such alloys exhibit sufficient resistance to corrosion, adequate mechanical characteristics, and acceptable biocompatibility (Ref 2). However, release of some toxic ions during wear and corrosion of alloys occurs after long implantation periods that crucially limits their medical application. In addition, there is weak bonding between metallic implants and human tissues (Ref 3).

The application of coating on metallic alloys has been used as a successful solution since decades to overcome these drawbacks. As the state of the art, hydroxyapatite (HA) has been proved and tested to be an excellent coating material for metallic implants, as it improves the biocompatibility, osteoconductivity, thermodynamic stability, and corrosion behavior of metallic implants (Ref 4, 5).

Numerous coating techniques are applied to coat metal implants. Non-oxide ceramic and metal alloy thin films are frequently manufactured by means of PVD processes. Magnetron sputter technique and pulsed laser deposition

✉ M. Blum
Matthias.Blum@ifkb.uni-stuttgart.de

¹ Institute for Manufacturing Technologies of Ceramic Components and Composites (IMTCCC), University of Stuttgart, Allmandring 7b, 70569 Stuttgart, Germany

² Refractories Ceramics and Building Materials Department, National Research Centre, El-Bohous Str, Cairo 12622, Egypt

are most common in orthopedic implant industry. Electrochemical and sol-gel deposition techniques are used to deposit HA coatings. Thermal spraying has been applied for decades to manufacture thick (in the range of 100 μm) calcium phosphate-based coatings such as HA and TCP on metal implant surfaces (Ref 6–11). Atmospheric plasma spraying is representing the industrial standard for this task, particularly recommended by the United States Food and Drug Administration (US FDA) (Ref 12–15).

Some studies show that the optimum HA coating thickness for efficiently enhancing osteogenesis for biomedical applications is 50–100 μm or less (Ref 16–18). Thinner coatings may regulate bone tissue metabolism for healing and for maintaining the mechanical properties of the alloy substrate (fracture and topography) (Ref 19).

Thermal spraying using suspensions is a feasible approach to spray coatings in a range of 10–50 μm and is under investigation since more than two decades (Ref 20). Especially high-velocity suspension flame spraying (HVSFS) has been proven to produce dense and well adherent calcium phosphate-based coatings like HA, TCP as well as bioglass layers (Ref 21, 22).

Bioactivity is evaluated through the generation of a bone-like apatite layer at the surface of an implant material after the material is immersed in simulated body fluid (SBF). Immersion in SBF is used to reflect the ability of a biomaterial to promote a direct physicochemical bond with the surrounding living tissue; the material's response can be considered a bioactivity rejoinder to mimic in vivo surface changes (Ref 23, 24). However, additional investigations are required to determine upregulation of bone-growth supporting proteins and cytokines as well as cell adhesion, proliferation and spreading. An in vitro evaluation of HA-coated Ti-6Al-4V via plasma spraying showed the generation of bone-like apatite particles on the surface of the HA coating (Ref 25–29). These results were confirmed by clinical tests on HA-coated dental implants and hip prostheses (Ref 30, 31). One of the first systematic SBF and in vitro cell growth studies on HVSFS sprayed HA coatings from nanopowder feedstock has been published in (Ref 32).

Most of the available hydroxyapatite used as a coating material is produced from chemical sources. However, chemically produced HA lacks some important trace elements that are found in natural human bones, such as Na^+ , Sr^{2+} , Mg^{2+} , and Si^{4+} ; this deficiency affects the hydroxyapatite's bioactivity behavior. On the contrary, bio-origin HA materials possess these trace elements as naturally occurring components; thus, they may offer additional benefits compared to chemically prepared hydroxyapatite. Fish waste is one possible natural source and has been investigated by Naga et al. (Ref 33) and others (Ref 34, 35). Nevertheless, implant materials from natural

sources also may contain undesired substances in alterable concentration. This has to be kept in mind if such a material is considered to be qualified for future biomedical applications.

In this study, a hydroxyapatite coating was deposited by means of a high-velocity suspension flame spray (HVSFS) process using a naturally derived nanocrystalline HA that we call biogenic HA (b-HA), dispersed in aqueous suspension. The initial powder consists of natural hydroxyapatite extracted from fish bones, which naturally contains all metabolic trace elements needed for enhancing bone formation. Experiments encompassed purified powder preparation, suspension development, and spray operation using the HVSFS process. In vitro investigations were conducted to evaluate the bioactivity potential of the produced Ti/Al alloys coated with hydroxyapatite.

Materials and Methods

Biogenic Hydroxyapatite Powder Preparation

Biogenic hydroxyapatite (b-HA) powder was extracted from fish bone skeletons according to the procedure described by Naga et al. (Ref 33). The obtained hydroxyapatite powder was ball-milled for 1 h at 300 rpm. The powder was sieved through a 200-mesh sieve, and the phase composition of the powder was examined by x-ray diffraction (Philips, PW 1730 x-ray diffractometer) with a Cu K_α target and Ni filter, with secondary monochromator. XRD patterns operated at 40 kV, 40 mA, scanning speed of 20° per min, and step size of 1° in the 2θ range from 15 to 60°. The surface morphology was investigated using scanning electron microscopy (Quanta FEG 250, Netherlands). Laser granulometry and transmission electron microscopy (TEM) at 200 kV (JEM-2100-HR Electron microscope, JEOL, Japan) were used to examine the particle size.

Suspension Feedstock Development

Three different dispersants (Zschimmer & Schwarz GmbH, Germany), namely KV9067, KV9068, and KV9069, were investigated to obtain a stable suspension for the thermal spraying. The produced suspensions were isopropanol-based with a solid HA content of 10% by weight, which we made good experience in previous investigations with and different percentages of dispersants (0.5%, 1%, and 2% by weight), as shown in Table 1.

A multistep milling and homogenization process was performed to optimize the size distribution of the HA powder and to fabricate stable suspensions. The suspensions were milled in an attritor until reaching a targeted

Table 1 Summary of the suspension recipes for the tested suspension variants (01–10) with different percentages of added dispersants.

Name	Isopropanol, g	HA, g	KV 9067	KV 9068	KV 9069
Suspension 01	300	30	0.5 wt. %
Suspension 02	300	30	1 wt. %
Suspension 03	300	30	2 wt. %
Suspension 04	300	30	...	0.5 wt. %	...
Suspension 05	300	30	...	1 wt. %	...
Suspension 06	300	30	...	2 wt. %	...
Suspension 07	300	30	0.5 wt. %
Suspension 08	300	30	1 wt. %
Suspension 09	300	30	2 wt. %
Suspension 10	300	30	1 wt. %	...	0.5 wt. %

particle size of about 5µm. On the one hand, this target value was chosen because from previous investigations it appeared, that HA particles larger than 5µm do not completely melt in the HVFS process. On the other hand, if the particles are getting too small, a higher coating porosity can be observed, this is mainly a consequence of the low inertia of the particles. The particle size distribution was measured with a laser granulometer Mastersizer 3000 (Malvern Instruments, Malvern, UK) and zeta potential were measured with a Zetasizer (Malvern Instruments, Malvern, UK). As will be explained in more detail in Sect. [Characterization of Designed Suspensions](#), suspension 2 was finally chosen for further spray experiments.

Experimental Procedure of Thermal Spraying Process

The spraying of the prepared hydroxyapatite suspension was performed with optimized parameter sets achieved from pre-studies on Ti plates and rods these parameters are shown in Tables 2 and 3, respectively.

The gas–oxygen ratio was set to sub-stoichiometric lambda ($\lambda = 0.78$), and the total gas volume was 300 standard liter per minute (slpm). For all coatings, a combustion chamber with a length of 22 mm and an expansion nozzle length of 78 mm was used. Grade 2 Ti plates and rods were coated in a preliminary study to work out

Table 2 Summary of spray parameters

Fuel gas/oxygen ratio, slpm:	90/210 ($\lambda = 0,78$)
Suspension feed rate, ml/min	40
Suspension atomizer gas, l/min	5
Combustion chamber geometry	22-8-78
Injection nozzle/diameter, mm	PM0.1/0.5 mm
Coating angle	90°
Simultaneous air cooling	2 nozzles, 4bar

appropriate spray parameters and then finally applied on US FDA-approved Ti-6Al-7Nb (TAN) rods (DePuy Synthes, USA) having a diameter of 4 mm and lengths of 10-15 mm. These rods were then used for in vitro investigations. Grit blasting was performed with corundum using F60 (212-300 µm) and F100 (106-150 µm) at 4 bar to activate substrate surfaces. Two plates with the same activation were sprayed simultaneously but at different distances from the torch (110 and 120 mm). Figure 1 shows the experimental setup of the spray system, which was operated at the University of Stuttgart.

A modified Top Gun torch (GTV Verschleißschutz, Luckenbach, Germany) capable of suspension spraying was used. A sample holder was used to mount the flat Ti samples, and a turning lathe was operated to manipulate the Ti rods. A simultaneous air cooling with a pair of adjustable nozzles was mounted at the torch head to cool the Ti substrates by an air jet (4 bar) during the spraying process. The substrate temperature was kept below 300 °C during the spray process to minimize risk of coating delamination induced by high thermal stresses. The spraying of the hydroxyapatite suspension was performed with optimized parameter sets achieved from pre-studies on Ti plates and rods according to the parameters given in Tables 2. The effect of preheating the substrates to approximately 200°C was also investigated. The results of the preliminary study were then transferred to the b-HA coatings on the US FDA-approved rods, which were designated as E1–E3. The parameter sets for specimens E1 and E2 were identical. E2 was added here as a control. The experimental parameters are summarized in Table 3.

The thicknesses of the HA coatings were examined by SEM coupled with energy-dispersive spectroscopy (EDS) (Quanta FEG 250, Netherlands) as well as by optical microscopy. Some rod segments were prepared as retain samples, and their surface roughness and coating were characterized (PST-MSE Perthometer, Mahr, Germany).

Table 3 Summary of the experimental procedures for plates and rods

Sample	Grainsize FEPA N°	Spray distance, mm	Sample Preheating, °C	N° of Spray cycles
Plate 2.1	F60	110	...	10
Plate 2.2	F60	120	...	10
Plate 2.3	F60	110	200	10
Plate 2.4	F60	120	200	10
Plate 2.5	F100	110	...	8
Plate 2.7	F100	110	200	10
Plate 2.8	F100	120	200	10
Rod 4.1	F100	110	...	10
Rod 4.2	F60	110	...	10
Rod 4.3	F100	120	...	10
Rod 4.4	F60	120	...	20
Rod E.1	F100	120	...	20
Rod E.2	F100	120	...	20
Rod E.3	F100	120	...	30

Pre-treatment of substrates was done by grit blasting with corundum, grain size is given as FEPA number. Rods E1 – E3 were US FDA-approved material and thus used for subsequent bioactivity studies

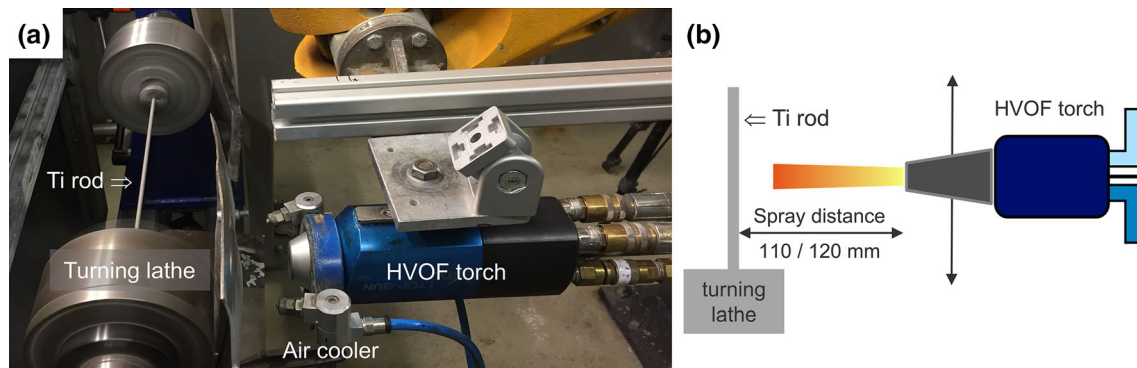


Fig. 1 (a) Experimental setup for HVSFS coating process at University of Stuttgart. (b) Sketch of the torch kinematic in case of the Ti rod coating procedure

Transfer to Demonstrator Screw

To demonstrate the capability of our process, the results from the rods were finally transferred to a commercially available dental implant screws from US manufacturer Dentis (Ref 32). Parts are fabricated from medical grade Ti with a diameter of 3.7 mm and a length of 14 mm and represent the root part of a tooth implant used in dental surgery (Dentis DSFM3714S) that is screwed into the maxillary bone (Fig. 2).

To meet the more complex screw geometry, the handling and torch kinematic during HVSFS spray process had to be adjusted, as outlined in Fig. 3. A special support had to be designed and constructed to hold and rotate the screw and owing to the high gas flux and thermal load, a windowed shield was required to minimize mechanical impact and thermal load during the spray process. Details of the experimental setup are shown in Fig. 3.

The first pass in front of the rotating screw was performed with a 90° angle (Pos.1) followed by each 5 cycles of 55°→90°→135°(Pos.2→Pos.1→Pos.3) and with a final 90° pass. The angles (55°, 135°) were not chosen symmetrically, because of the different flank angles of the screw. The spray distance was kept constant at 120 mm; the other torch parameters were chosen according to Table II.

Bioactivity Test in SBF Solution

Corrected SBF (c-SBF) solution was prepared in accordance with the protocol of Kokubo and Takadama (Ref 37), which is composed of 142.0 mM Na⁺, 5.0 mM K⁺, 1.5 mM Mg²⁺, 2.5 mM Ca²⁺, 147.8 mM Cl⁻, 4.2 mM HCO³⁻, 1.0 mM HPO₄²⁻, and 0.5 mM SO₄²⁻ dissolved in 1000 ml deionized water. The prepared solution was buffered with Tris and HCl to adjust pH at 7.4. The HA-coated Ti rods were immersed in 100 ml SBF at 37°C for 28 days,

Fig. 2 Details of the Ti medical screw demonstrator part (Manufacturer: Dentis, La Palma CA 90623, USA). (a) Mounted screw body before coating. (b) Manufacturer data (Ref 36).

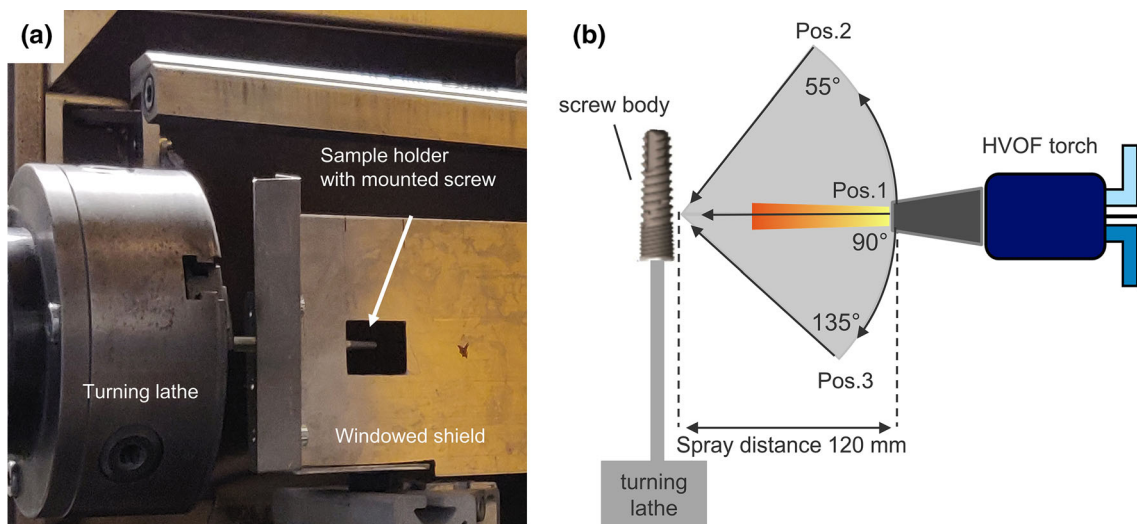
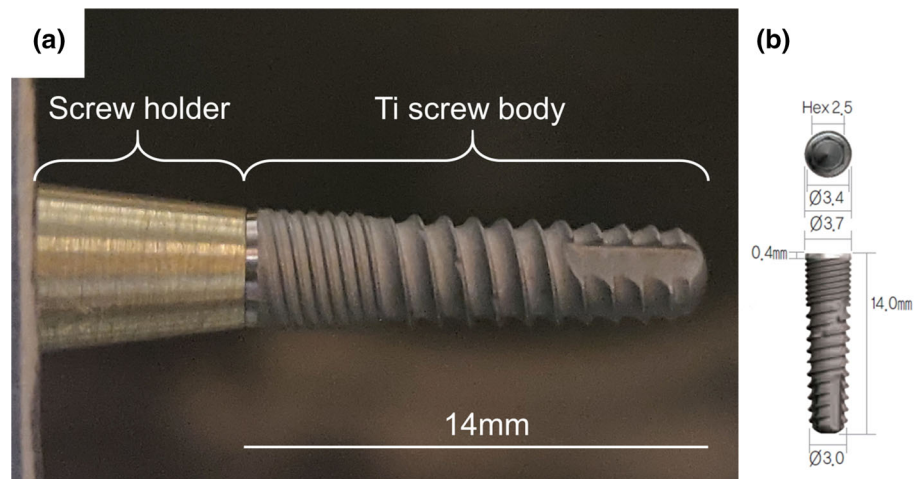


Fig. 3 Experimental setup for screw coating: (a) Setup in spray booth, (b) Sketch of the HVFS coating process, see more details in text.

with a solid/liquid ratio of 0.6 g/L. After being immersed in the SBF solution for the following amount of time (1,7,14, 21, and 28 days), the rods were dried at 100°C for 1 day, and analyzed by inductively coupled plasma–optical emission spectrometry (ICP–OES) (5100 ICP–OES torch, Agilent, Australia). For evaluation of the concentration of the calcium, phosphorus, and titanium ions, each solution measurement was conducted three times, and the average value was calculated. Furthermore, the microstructure of the apatite layer on the studied coated rods was investigated by an SEM device (Quanta FEG 250, Netherlands) with an attached energy dispersive x-ray spectroscopy EDS unit. The phase composition for the surface layer of the coated rod after immersion in SBF solution up to 28 days was examined via thin film XRD analysis (XPert Pro. PANalytical, target Cu-K α with second monochromator K ν = 45 mA; 4 Netherlands).

Biodegradation Estimation

The in vitro degradation was estimated by assessing the weight loss (WL) percentage of the HA-coated Ti rods in the SBF solution at pH 7.4 and 37°C. The coated rods were weighed and soaked in 100 ml SBF for different soaking periods (1, 3, 7, 14, 21, and 28 days). After each immersion period, the coated rods were accurately weighed after being dried at 100°C for 1 day. The biodegradability test was performed on three samples, and the mean value was calculated to ensure the test results’ precision (Ref 38). The change in the pH of the SBF solution, as a function of the previously detected immersion time of the incubated coated samples, was measured using a pH meter (Jenway Model 3510 pH/mV/Temperature Meter, United Kingdom).

Results and Discussion

Characterization of Naturally Derived Hydroxyapatite Powders

The XRD pattern of the hydroxyapatite powder calcined at 900°C for 3 h (Fig. 4), demonstrated the existence of HA as a pure phase without the presence of any secondary phases, ICDD (JCPDS) standard cards 009-0432. On the one hand, prior studies stated that HA can be obtained with high purity and stability at 900°C (Ref 34, 39). Accordingly, 900°C was selected to be the calcination temperature. On the other hand, some studies indicated that increasing the calcination temperature above 900°C led to the formation of a minor amount of β -tricalcium phosphate (β -TCP) (Ref 40–42).

Figure 5a shows the SEM images of the as-prepared HA (without any treatment). The image obviously shows that the prepared HA powder was quite fine, having a submicron particle size. However, a strong tendency of particle agglomeration can be easily identified from the image. Such agglomeration tendency was confirmed by the laser granulometry measurements of the initial powder particles (Fig. 5b).

The prepared HA exhibited a trimodal distribution, with maxima at approximately 0.1, 1, and 90 μm . The TEM examination revealed that the particle size of the calcined HA powder varied between nanometers and micrometers (Fig. 5c). This result matched those obtained from the laser granulometry measurements.

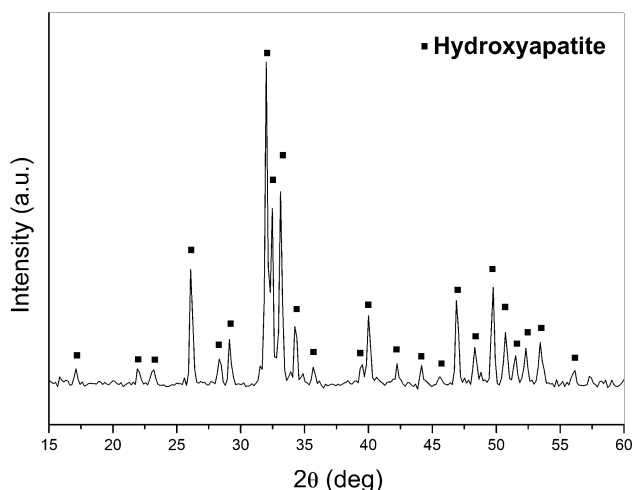


Fig. 4 XRD pattern of the prepared HA powder after 3 h heat treatment at 900°C.

Characterization of Designed Suspensions

After 4 h of ball milling, the particle size distribution and the Zeta potentials of the investigated suspensions were measured and compared. Results for all 10 suspensions are summarized in Table 4. In most cases, Zeta potential values near ± 30 mV show low particle agglomeration tendency, thus promoting sufficient stability of the ceramic suspension. For suspension spraying, this is particularly important, as agglomeration can cause clogging within the torch injector system, leading to an instable coating process. As discussed earlier, particle size distribution close to a D_{90} of 5 μm is preferred. From the values shown in Table 4, suspension #2 was finally chosen for the coating experiments, as it showed optimum particle size and overall processability.

Characterization of Hydroxyapatite Coating Used for Metallic Ti Implants Coated by Thermal Spraying Technique

Microstructure and Phase Composition

An example of the achieved coating structure is shown in Fig. 6. The coatings appeared dense and had small cracks arising from residual tensile stresses. Deposition efficiency was significantly higher on the plates, which can be easily explained by the small diameter size of the rod that caused substantial powder loss by overspraying. Deposition efficiencies are summarized in Table 5 and are calculated according to DIN EN ISO 17836 (Ref 43). Compared to the rod dimension, the spray spot diameter is significantly larger; thus a significant fraction of the particles cannot hit the surface. Some uncertainty is also evident due to sedimentation effects of the suspension that occurs during the spray process.

The micrographs indicate a well-formed adhesion bond between the coating and the Ti substrate. Therefore, pretreatment with F100 is sufficient for good mechanical anchoring of the spray coating. Figure 6 shows an example of the thickness difference in the coatings on the Ti plates and rods. Identical grit blasting and spray parameters were used (F60, 110 mm). Based on the spraying results, rod samples E1, E2, and E3 were sprayed and used in further investigation.

The XRD pattern of the surface of the Ti substrates coated with b-HA displayed typical profiles for weakly crystalline hydroxyapatite and β -tricalcium phosphate (β -TCP) phases together with an amorphous calcium phosphate (ACP), which manifests itself by the elevated background intensity between 25 and 35 degrees 2 theta. (Fig. 7). The presence of the HA and β -TCP phases corresponded to the ICDD (JCPDS) standard cards 009-0432

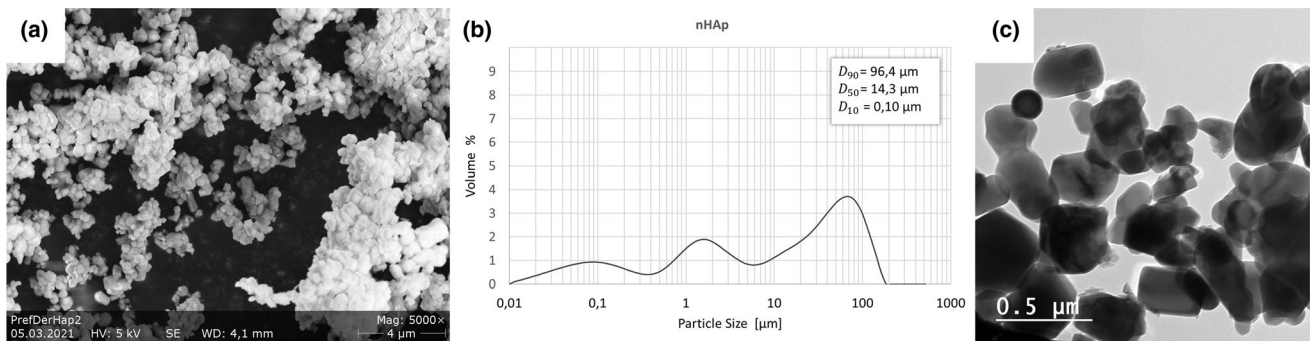


Fig. 5 (a) SEM images of as-prepared fish bone HA powder, (b) Laser granulometry pattern of the as-prepared HA powder, (c) TEM image of individual powder particles.

Table 4 Summary of the particle size measurement and Zeta-potential of the suspension recipes for the tested suspension variants (01–10) after 4 h of milling

Name	D ₁₀	D ₅₀	D ₉₀	Zeta-Potential
Suspension 01	1.61	4.09	11.94	36.8
Suspension 02	1.23	2.79	5.38	45.1
Suspension 03	1.41	3.39	8.68	39.1
Suspension 04	1.37	3.17	7.48	35.3
Suspension 05	1.39	3.30	8.23	36.9
Suspension 06	1.40	3.39	8.73	47.2
Suspension 07	1.70	3.60	7.48	18.0
Suspension 08	1.92	3.93	7.68	8.3
Suspension 09	2.27	4.76	9.08	3.8
Suspension 10	1.42	3.34	7.97	44.3

Suspension #2 was chosen for coating application.

and 32-0176, respectively. The presence of ACP can be explained by the fact that crystallization is hindered due to a high cooling rate during particle impact, that is also fostered by the small particle diameters that are present in suspension spraying. As mentioned earlier, the substrate temperature had to be kept below 300°C to avoid high thermal stresses. Higher crystallization during HVSF

deposition can be only expected at significantly higher temperatures ($\approx 450^\circ\text{C}$); this has been extensively discussed in (Ref 32). There, higher crystallization rates have been achieved by the use of a thermally insulating TiO₂ bond coat.

Coating Morphology

SEM images of the coating morphology of the biogenic hydroxyapatite coating samples E1, E2, and E3 (sprayed on TAN rods) are shown in Fig. 8(a), (b) and (c). Layer thicknesses were derived from cross section images in optical microscopy and in SEM. The results indicate somewhat different thickness values, with E3 having the largest layer thickness (32 μm), an E1 and E2 having coating thicknesses of 27 μm and 23 μm, respectively (averaged values). These findings are attributed to the spray cycles applied to E3 (30 cycles) in comparison to that for E1 and E2 (20 cycles). Results of optical microscope examinations are summarized in Table 6. Variations were identified between the different rods (E1, E2, and E3) but not between the segments of a single rod. Some researchers stated that the optimal coating thickness of biocompatible HA has to be 50–100 μm or even less to improve its osteogenesis function for biomedical implementation (Ref

Fig. 6 Representative examples of SEM images of b-HA coating on plate 2.1 (a) and rod 4.4 (b).

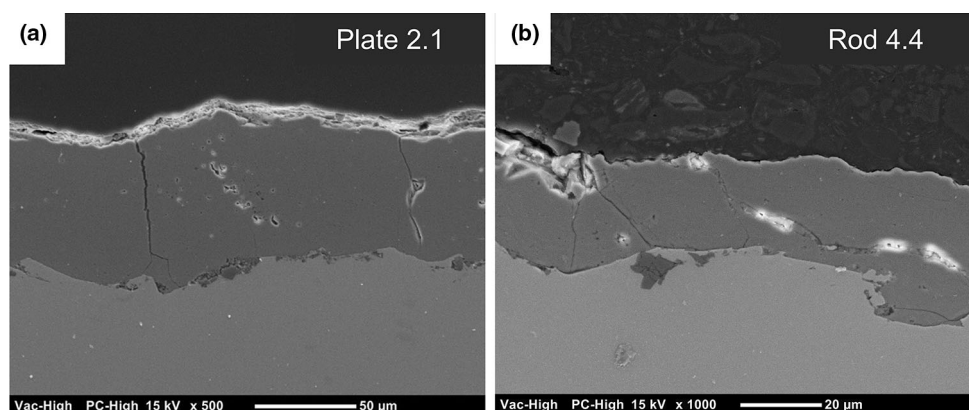
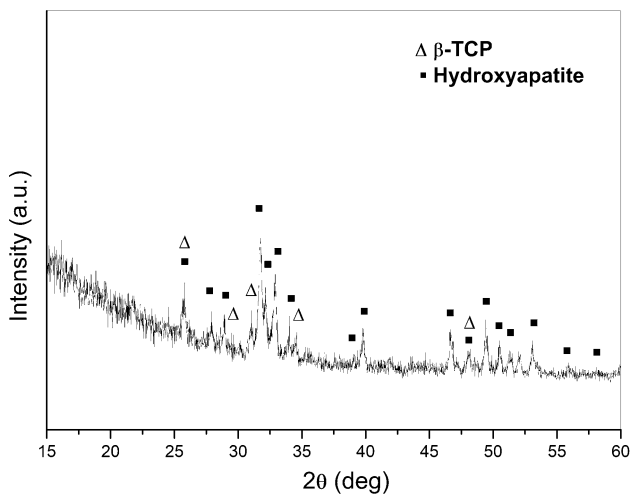


Table 5 Deposition efficiency of the different spray parameters DIN EN ISO 17836

Plate	Deposition efficiency, %	Rod	Deposition efficiency, %
Plate 2.1	70	Rod 4.1	5
Plate 2.2	64	Rod 4.2	6
Plate 2.3	73	Rod 4.3	7
Plate 2.4	69	Rod 4.4	11
Plate 2.5	58	Rod E.1	19
Plate 2.7	73	Rod E.2	14
Plate 2.8	65	Rod E.3	14

**Fig. 7** Thin layer XRD pattern of Ti E2-rod surface coated with b-HA

16–18). Also thinner coatings enable the regulation of bone tissue metabolism for the healing process. Moreover, they maintain the mechanical properties of the alloy substrate in terms of fracture and topography (Ref 19). The proposed

HA coating thickness fulfills these requirements. The microstructural features of the coating surface of the Ti implants indicate that the produced HA coatings layer is uniform and exhibit low porosity and rare appearance of cracks.

Surface roughness has a significant positive influence on bone growth. Rough surfaces offer many advantages, including support for good stability between the implant and the surrounding bone tissue, which accelerates bone formation and healing. Such process is achieved by increasing the amount of contact area and supporting blood clot retention during the initial stage of healing (Ref 44).

Table 6 represents the average surface roughness (Ra) of the grit blasted Ti substrate surface before (TAN Rod) and after (Rods E1-E3) being coated with the b-HA ceramic coating. The results revealed that the coated samples possess moderate roughness ranging within the recommended values (1–2 μm), where bone tissue formation is promoted (Ref 45). Many studies show that micro-roughened surfaces positively impact initial blood cell–implant interactivity (Ref 46) and osteoblast proliferation (Ref 47). Surface topography and the fractal nature of the surfaces

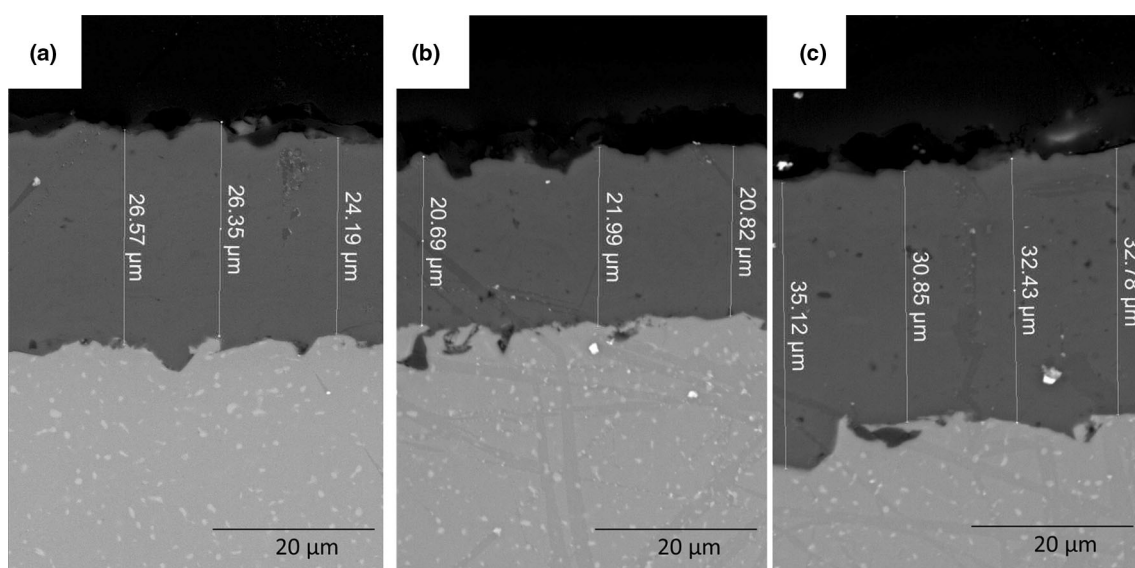
**Fig. 8** Cross sectional SEM images of coatings on rods E1 (a), E2 (b) and, E3 (c) with measured coating thicknesses labeled in the images.

Table 6 Summary of surface roughness and coating thickness of coated rods

Sample	Ra \pm SD, μm	Rz \pm SD, μm	Layer thickness \pm SD, μm
TAN rod	1.4 \pm 0.07	10.7 \pm 0.8	0 (prior to coating)
Rod E.1	1.28 \pm 0.09	9.02 \pm 0.91	26.6 \pm 2.6 (27)
Rod E.2	1.48 \pm 0.11	10.64 \pm 0.83	22.8 \pm 1.9 (23)
Rod E.3	1.39 \pm 0.12	9.43 \pm 1.01	32.5 \pm 2.3 (32)

Thickness values in brackets refer to the rounded values. Ra and Rz values of the TAN rod refers to grit-blasted surface prior to coating.

has a considerable effect on osteoconduction and a rough surface yields acceptable results during implantation studies (Ref 48–50). It is well known that the roughness values depend on many factors, such as the applied deposition technique, the dimensions of the HA powder, and the roughness of the used Ti substrate (Ref 51).

Microstructure and Coating Thickness of the Demonstrator

Figure 9 reveals the appearance of the coated demonstrator screw body. In Fig 9(a), a macro-image photography of the coated screw is shown. The coating thickness was in the range of 19 μm (19.39 ± 1.48) after applying 16 torch passes. Fig. 9(b) shows stitched microscope images of the cross section of the entire screw. In Fig 10(a) and (b) details of Fig. 9 are shown. The coating accurately follows the screw contour geometry with an evenly distributed coating thickness, and it also covers the steep slopes of the thread.

In Vitro Bioactivity Evaluation of Coated Rod Samples

The bioactivity behavior of the HA/Ti composite samples fabricated via the high-velocity suspension flame spray technique was evaluated by immersing the coated samples

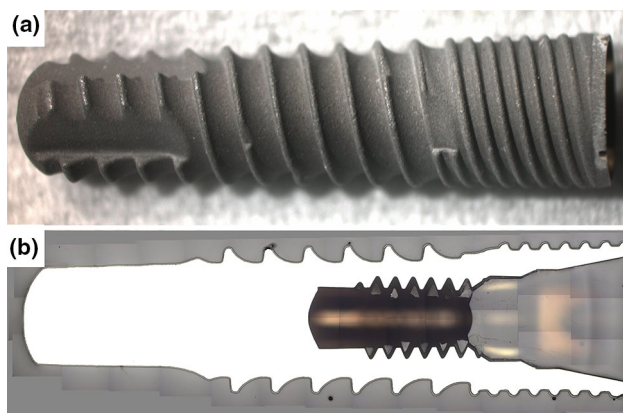


Fig. 9 (a) Photography of the coated screw. (b) Stitched images of the cross section of the coated screw, reproduced from optical microscope images.

(E1, E2, and E3) in SBF for up to four weeks. The surface morphology of the HA/Ti samples before and after being soaked in the SBF solution for four weeks was estimated by SEM (Fig. 11). A layer of fine particles developed and covered the surface of the samples (E1–E3). The generation of the apatite layer over the HA/Ti surface was based on the presence of negatively charged OH^- and PO_4^{3-} ion groups in the HA structure. These groups can attract positive Ca^{2+} ions from the surrounding SBF solution. Accordingly, the surface gained a positive charge, which enhanced the attraction of the negatively charged OH^- and PO_4^{3-} ions from the surrounding SBF solution. Moreover, it should be mentioned that SBF is close to supersaturation with HA; hence, the ion product requires only minor addition of Ca^{2+} and PO_4^{3-} ions to yield precipitation of HA. The previous reaction was repeated several times, leading to the precipitation of an HA layer on the surface of the samples (Ref 52). The SEM results suggest that the coated samples possess bioactive characteristics, based on their chemical behavior.

Energy dispersive x-ray spectroscopy (EDS) analysis was performed to confirm the composition of the apatite layer formed on the surface of the HA/Ti alloy composites after they were immersed in the SBF solution for four weeks. The EDS analysis findings reflect the estimated molar ratio for Ca and P ions as essential constituents of the formed HA layer. The detected Ca–P molar ratio were in the range of 1.61 to 1.66 (E1 = 1.61, E2 = 1.66, E3 = 1.61). This indicates the formation of a slightly Ca-deficient HA in case of E1 and E3 and a near stoichiometric Ca–P ratio (which is 1.67) for E2.

The formation of the apatite layer was also confirmed through ICP analysis (refer to Fig. 12). The average concentration of the Ca^{2+} and PO_4^{3-} ions released from the coatings keeps rather constant throughout the first 3 weeks but significantly decreased after the fourth week of incubation in the SBF solution (Fig. 12). This is presumably caused by ion consumption due to the formation of an apatite top layer (Ref 53). Results confirm a good chemical stability of the coatings, with a low Ca^{2+} and PO_4^{3-} ion concentration during the initial weeks of immersion and a sharp drop after the fourth week which is in good agreement with other studies (Ref 23). The ICP analysis also

Fig. 10 Detail of Fig. 9 (optical microscope) showing thickness distribution of the coated screw in axial (a) and radial (b) cross section. A detailed image of the coating from (b) is shown (c).

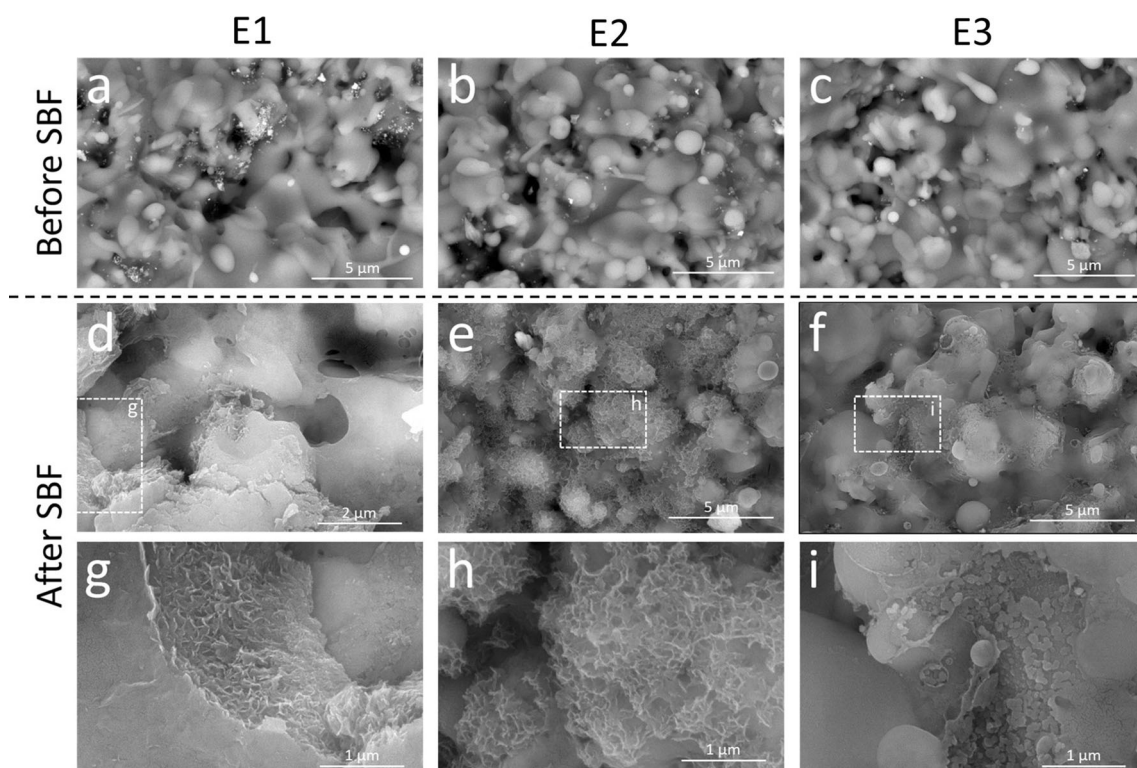
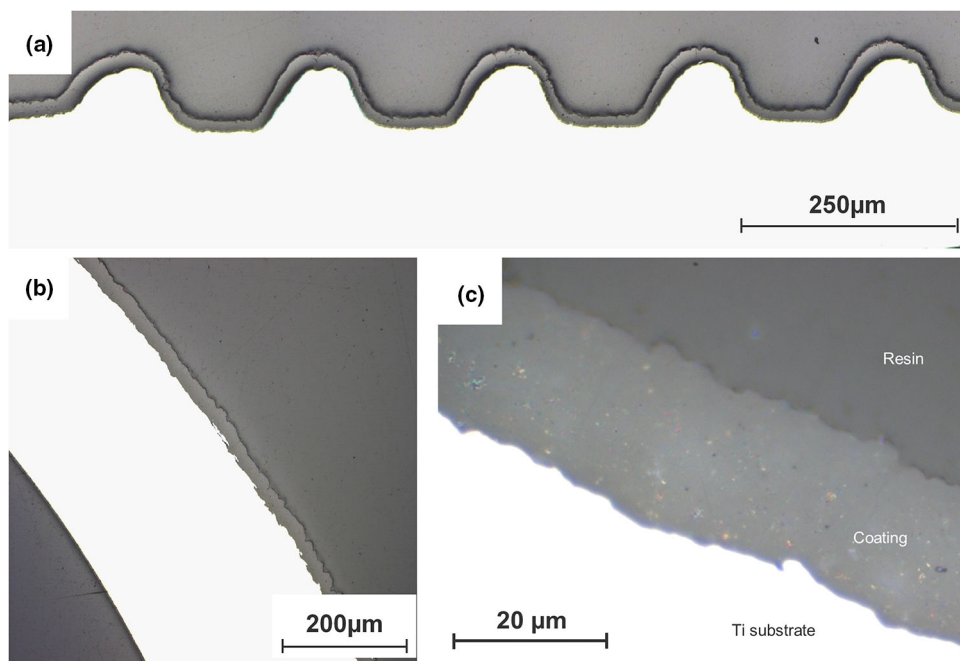


Fig. 11 SEM micrographs for the surface of the fabricated HA coatings developed on samples E1, E2, and E3: (a)–(c) before and (d)–(f) after four-week immersion in SBF; (g)–(i) show details of the

insets in micrographs (d)–(f), respectively. Note that insert (g) is only partially visible in (d).

confirmed the absence of any Ti ion throughout the studied immersion times, at least, it was below the detection limit of the used ICP device which is less than 0.01 mg/l. The obtained results are in good agreement with Suito et al.

(Ref 54) and Singh et al. (Ref 55) who found, that the concentration of the Ti ions after incubation in SBF solution up to 28 days is below the detection limit at pH values

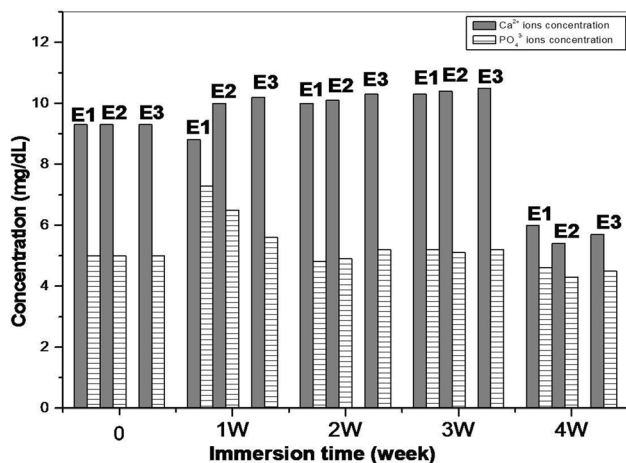


Fig. 12 Mean Ca^{2+} and PO_4^{3-} ion concentration (mg/dL) for the three HA coatings E1, E2, E3 during the four-week immersion in SBF solution determined using ICP analysis.

of 5.0 to 7.4. Higher concentrations could only be detected on pH values below 3.

Inflammation may happen after metallic alloy implantation due to material degradation and the release of the ions of the implanted alloys, given that most metallic materials undergo electrochemical corrosion in fluid media under certain conditions. Ti and Ti- alloys are corrosion-resistant in air and biological media due to the formation of a dense oxide outer layer of a few nm thickness (Ref 56). However, this formed oxide film can take damage due to mechanical stress (Ref 57). In this case, a dense HA coating with a low diffusion coefficient may help to reduce Ti ion release, especially after a long period of implantation. Figure 13(a) depicts the biodegradation behavior of the HA/Ti composite samples (E1–E3) after immersion in the SBF solution for 4 weeks. The E3 sample showed a significantly higher WL percentage up to the third week with a sharp drop in the fourth week. This effect was less pronounced in case of E1 and E2 coating. At the end of the fourth week, notably low degradability values (0.060%, 0.048%, and 0.053%) were detected for all three samples E1, E2, E3. The high WL percentages observed for the E1 and E3 samples during the first three weeks (Fig. 13a) showed that the dissolution rate of the HA coating was higher than the rate of the apatite formation. With the increase in the immersion time, the WL percentages decreased, which indicated the formation of the apatite layer. The abovementioned results were confirmed by the results given in Fig. 12, which show that both the calcium and phosphorus ion concentrations decreased during the fourth week due to the formation of the apatite layer. We believe that the degradability behavior is affected mainly by the high amount of amorphous phase, this was also found in the corresponding study (Ref 32) where a

quantitative analysis was performed. Also the presence of the β -TCP phase as a secondary phase contributes to a higher solubility and thus precipitation of apatite. (Ref 58, 59) The obtained results indicate that WL seems to be influenced by coating layer thickness, showing higher WL values at higher thickness values. This is especially obvious in the second and third week of immersion (weight loss in third week: E2 = 0.05%; E1 = 0.15%; E3 = 0.35% and thickness: E2 = 23 μm ; E1 = 27 μm ; E3 = 32 μm).

Figure 13(b) demonstrates the pH measurements against immersion time in the SBF solution. The results revealed that the pH values for E1, E2 and E3 had comparable values: first week (7.54, 7.50 and 7.53 for E1, E2 and E3, respectively) and last week (7.44, 7.43 and 7.47 for E1, E2 and E3, respectively) with a slight increase during the 1st and 2nd week and a decrease in the 3rd and 4th week. This decrease may be attributed to the formation of an apatite layer in the 3rd and 4th week during immersion. The formation of the apatite would then increase the consumption of the $(\text{OH})^-$ group from the SBF solution, thus lowering the pH values to levels similar to those of the physiological human blood (Fig. 13b) (Ref 60). The pH measurement results were consistent with the ICP analysis and degradation results (Figs. 12 and 13a).

Conclusion

The suspension spray technique allows the fabrication of thin and dense coatings with thickness values in the range of 23–33 μm and roughness values in the range of $R_z = 9 - 11 \mu\text{m}$, that fulfill the biomedical requirements reported in the literature. Moreover, the coatings displayed sufficient chemical stability, as indicated by their detected low biodegradability behavior upon immersion in SBF media for up to four weeks.

No spalling of the HA coating was detected during cutting, embedding and polishing operations during preparation of the samples for microscopic imaging. Some vertical cracks could be found within the coatings on flat samples and rods. However, on the TAN rods and the demonstrator screws we were able to further optimize the spray process and fabricate a crack free and well adherent, dense and evenly distributed b-HA coating. It demonstrates the capability of the spray process to be adapted to real medical components.

The in vitro study indicates sufficient bioactivity of the composites, as they formed a bioactive layer composed mainly of HA and a minor β -TCP phase. The pH value observed after immersion in SBF for four weeks was comparable to standard physiological pH values. No reactions of the Ti alloy with the body fluid environment was found, which we attribute to the dense b-HA coating

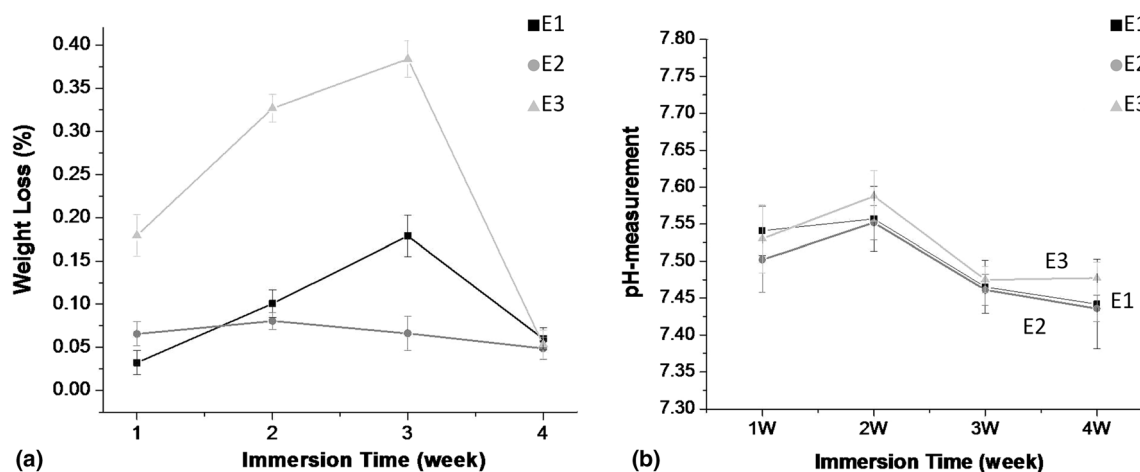


Fig. 13 (a) Weight loss (%) of the studied HA/Ti composite samples after four-week immersion in SBF solution, and (b) pH measurement after four-week immersion in SBF solution.

structure. The results are in good agreement with an earlier study that investigated coatings fabricated by employing synthetic nanosized HA and sprayed also using HVFS (Ref 32).

Our findings suggest the use of low-cost biogenic hydroxyapatite extracted from fish bones as an appropriate starting material for suspension fabrication and subsequent spraying using thermal spray coating processes. For the completion of the present study, we plan to carry out cell culture studies to examine the cell viability and assess the cytotoxicity of the HA coating. This *in vivo* study will be also implemented in further investigations.

Acknowledgments This work was financed by the Science & Technology Development Fund (STDF), Egypt (German-Egyptian Research Fund (GERF) Projects program), Project ID 23036. Our study did not involve human subjects.

Funding Open Access funding enabled and organized by Projekt DEAL.

Declarations

Conflict of interest The authors declare that they have no conflict of interest.

Open Access This article is licensed under a Creative Commons Attribution 4.0 International License, which permits use, sharing, adaptation, distribution and reproduction in any medium or format, as long as you give appropriate credit to the original author(s) and the source, provide a link to the Creative Commons licence, and indicate if changes were made. The images or other third party material in this article are included in the article's Creative Commons licence, unless indicated otherwise in a credit line to the material. If material is not included in the article's Creative Commons licence and your intended use is not permitted by statutory regulation or exceeds the permitted use, you will need to obtain permission directly from the copyright holder. To view a copy of this licence, visit <http://creativecommons.org/licenses/by/4.0/>.

References

1. W.S.W. Harun, R.I.M. Asri, A.B. Sulong, S.A.C. Ghani and Z. Ghazalli, Hydroxyapatite-based coating on biomedical implant, *Advances in Composite Nanomaterials, Biomedical Applications and its Technological Facets*. J. Thirumala Ed., In Tech, Croatia, 2018, p 69–88
2. R.C. Rocha, A. Gustavo de Sousa Galdino, S. Nicodemos da Silva, M.L. Pereira Machado, Surface, Microstructural, and Adhesion Strength Investigations of a Bioactive Hydroxyapatite-Titanium Oxide Ceramic Coating Applied to Ti-6Al-4V Alloys by Plasma Thermal Spraying, *J. Mater. Res. Technol.*, 2018, 21(4)
3. V.-T. Nguyen, T.-C. Cheng, T.-H. Fang and M.-H. Li, The Fabrication and Characteristics of Hydroxyapatite Film Grown on Titanium Alloy Ti-6Al-4V by Anodic Treatment, *J. Mater. Res. Technol.*, 2020, 9(3), p 4817–4825.
4. M. Rahman, Y. Li and C. Wen, HA Coating on Mg Alloys for Biomedical Applications: A Review, *J. Magnes. Alloys*, 2020, 8(3), p 929–943.
5. R.B. Heimann and H.D. Lehmann, *Bioceramic Coatings for Medical Implants Trends and Techniques*, Wiley-VCH, Hoboken, 2015.
6. W.S.W. Harun, R.I.M. Asri, J. Alias, F.H. Zulkifli, K. Kadirgama, S.A.C. Ghani and J.H.M. Shariffuddine, A Comprehensive Review of Hydroxyapatite-Based Coatings Adhesion on Metallic Biomaterials, *Ceram. Inter.*, 2018, 44, p 1250–1268.
7. C. Massaro, M. Baker, F. Cosentino, P. Ramires, S. Klose and E. Milella, Surface and Biological Evaluation of Hydroxyapatite-Based Coatings on Titanium Deposited by Different Techniques, *J. Biomed. Mater. Res.*, 2001, 58, p 651–657.
8. E. Mohseni, E. Zalnezhad and A. Bushroa, Comparative Investigation on the Adhesion of Hydroxyapatite Coating on Ti-6Al-4V Implant: A Review Paper, *Inter. J. Adhes. Adhes.*, 2014, 48, p 238–257.
9. R.I.M. Asri, W.S.W. Harun, M.A. Hassan, S.A.C. Ghani and Z. Buyong, A Review of Hydroxyapatite-Based Coating Techniques: Sol-Gel and Electrochemical Depositions on Biocompatible Metals, *J. Mech. Behav. Biomed. Mater.*, 2016, 57, p 95–108.
10. M. Chambard, O. Marsan, C. Charvillat, D. Gossin, P. Fort, C. Rey, F. Gitzhofer and G. Bertrand, Effect of the Deposition Route on the Microstructure of Plasma-Sprayed Hydroxyapatite Coatings, *Surf. Coat. Technol.*, 2019, 371, p 68–77.

11. Q.Y. Chen, Y.L. Zou, X. Chen, X.B. Bai, G.C. Ji, H.L. Yao, H.T. Wang and F. Wang, Morphological, Structural and Mechanical Characterization of Cold Sprayed Hydroxyapatite Coating, *Surf. Coat. Technol.*, 2019, **357**, p 910–923.
12. “Guidance Document for Testing Orthopedic Implants with Modified Metallic Surfaces Apposing Bone Or Bone Cement,” FDA-2020-D-0957, Food and Drug Administration, 1994
13. “510(K) Information Needed for Hydroxyapatite Coated Orthopedic Implants,” FDA-2020-D-0957, Food and Drug Administration, 1997
14. C.C. Berndt, M.F. Hasan, U. Tietz and K.P. Schmitz, A review of hydroxyapatite coatings manufactured by thermal spray, *Advances in Calcium Phosphate Biomaterials*. B. Ben-Nissan Ed., Springer, New York, 2014, p 267–329
15. J.A. Hermann-Munoz, J.A. Rincon-Lopez, G.A. Clavijo-Mejia, A.L. Giraldo-Betancur, J.M. Alvarado-Orozco, A. De Vizcaya-Ruiz and J. Munoz-Saldana, Influence of HVOF Parameters on HAp Coating Generation: An Integrated Approach Using Process Maps, *Surf. Coat. Technol.*, 2019, **358**, p 299–307.
16. A.K. Lynn and D.L. DuQuesnay, Hydroxyapatite-Coated Ti-6Al-4V: Part 1: The Effect of Coating Thickness on Mechanical Fatigue Behavior, *Biomaterials*, 2002, **23**(9), p 1937–1946.
17. M. Svehla, P. Morberg, W. Bruce, B. Zicat and W.R. Walsh, The Effect of Substrate Roughness and Hydroxyapatite Coating Thickness on Implant Shear Strength, *J. Arthroplasty*, 2002, **173**, p 304–311.
18. H. Li, R. Zhu, L. Sun, Y. Xue, Z. Hao, Z. Xie, X. Fan, H. Fan, Effect of Thickness of HA-Coating on Microporous Silk Scaffolds Using Alternate Soaking Technology, *BioMed Res. Int.*, 2014, **2014**, Article ID 637821
19. D. Juliadmi, V.R. Fauzi, G. Gunawarman, H. Nur and M.H. Idris, Hydroxyapatite Coating on Titanium Alloy Ti-6Al-4V with Electrophoretic Deposition (EPD) for Dental Root Application, *Int. J. Adv. Sci. Eng. Inf. Tech.*, 2017, **7**(6), p 2152–2158.
20. E. Bouyer, F. Gitzhofer and M.I. Boulos, The Suspension Plasma Spraying of Bioceramics by Induction Plasma, *JOM*, 1997, **49**, p 58–62.
21. G. Bolelli, D. Bellucci, V. Cannillo, R. Gadow, A. Killinger, L. Lusvardi, P. Mueller and A. Sola, Comparison Between Suspension Plasma SPRAYED and High Velocity Suspension Flame Sprayed Bioactive Coatings, *Surf. Coat. Technol.*, 2015, **280**, p 232–249.
22. D. Bellucci, G. Bolelli, V. Cannillo, R. Gadow, A. Killinger, L. Lusvardi, A. Sola and N. Stiegler, High Velocity Suspension Flame Sprayed (HVSFS) Potassium-Based Bioactive Glass Coatings With and Without TiO₂ Bond Coat, *Surf. Coat. Technol.*, 2012, **206**, p 3857–3868.
23. Y.W. Gu, K.A. Khor and P. Cheang, In Vitro Studies of Plasma-Sprayed Hydroxyapatite/Ti-6Al-4V Composite Coatings in Simulated Body Fluid (SBF), *Biomaterials*, 2003, **24**(9), p 1603–1611.
24. C. Wu and Y. Xiao, Evaluation of the In Vitro Bioactivity of Bioceramics, *Bone Tissue Regen. Insights*, 2009, **2**, p 25–29.
25. P. Ducheyne, L.L. Hench, A. Kagen II., M. Martens, A. Bursens and J.C. Mulier, Effect of Hydroxyapatite Impregnation on Skeletal Bonding of Porous Cated Implants, *J. Biomed. Mater. Res.*, 1980, **14**, p 225–237.
26. R.G. Geesink and N.H. Hoefnagels, Six-Year Results of Hydroxyapatite-Coated Total Hip replacement, *J Bone Joint Surg Br.*, 1995, **77**(4), p p534–547.
27. J. Karrholm, H. Malchau, F. Snorrason and P. Herberts, ‘Micromotion of Femoral Stems in Total Hip Arthroplasty—a Randomized Study of Cemented, Hydroxyapatite-Coated, and Porous Coated Stems with Roentgen Stereophoto-Grammetric Analysis, *J. Bone Joint Surg.*, 1994, **76A**, p 1692–1705.
28. S.W.K. Kweh, K.A. Khor and P. Cheang, An In Vitro Investigation of Plasma Sprayed Hydroxyapatite (HA) Coatings Produced with Flame-Spheroidized Feedstock, *Biomaterials*, 2002, **23**(3), p 775–785.
29. P. Habibovic, F. Barrere, C.A. Van Blitterswijk, K. de Groot and P. Layrolle, Biomimetic Hydroxyapatite Coating on Metal Implants, *J. Am. Ceram. Soc.*, 2002, **85**(3), p 517–522.
30. T.M. Lee, B.C. Wang, Y.C. Yang, E. Chang and C.Y. Yang, Comparison of Plasma-Sprayed Hydroxyapatite Coatings and Hydroxyapatite/Tricalcium Phosphate Composite Coatings: In Vivo Study, *J. Biomed. Mater. Res.*, 2001, **55**(3), p 360–367.
31. C. Faldini, A. Moroni and S. Giannini, Hydroxyapatite Coated Total Hip Prostheses: A Long-term, Prospective, Randomized Study of 50 consecutive cases, *Key Eng. Mater.*, 2002, **218**(2), p 491–493.
32. G. Bolelli, D. Bellucci, V. Cannillo, L. Lusvardi, A. Sola, N. Stiegler, P. Müller, A. Killinger, R. Gadow, L. Altomare and L. De Nardo, Suspension Thermal Spraying of Hydroxyapatite: Microstructure and In Vitro Behaviour, *Mater. Sci. Eng. C*, 2014, **34**, p 287–303.
33. S.M. Naga, H.F. El-Maghraby, E.M. Mahmoud, M.S. Talaat and A.M. Ibrahim, Preparation and Characterization of Highly Porous Ceramic Scaffolds Based on Thermally Treated Fish Bone, *Ceram. Int.*, 2015, **41**, p 15010–15016.
34. M. Akram, R. Ahmed, I. Shakir, W.A. Wan Ibrahim and R. Hussain, Extracting Hydroxyapatite and its Precursors from Natural Resources, *J. Mater. Sci.*, 2014, **49**, p 1461–1475.
35. M. Bas, S. Daglilar, N. Kuskonmaz, C. Kalkandelen, G. Erdemir, S.E. Kuruca, D. Tulyaganov, T. Yoshioka, O. Gunduz, D. Ficai and A. Ficai, Mechanical and Biocompatibility Properties of Calcium Phosphate Bioceramics Derived from Salmon Fish Bone Wastes, *Int. J. Mol. Sci.*, 2020, **21**, p 8082.
36. <https://dentisusa.com/wp-content/uploads/2020/08/s-Clean-Implant-System.pdf> last Accessed from 13 Sep 2021
37. T. Kokubo and H. Takadama, How Useful is SBF in Predicting In Vivo Bone Bioactivity?, *Biomaterials*, 2006, **27**(15), p 2907–2915.
38. S.K. Motwani, S. Chopra, S.K. Talegaonkar, K. Kohli, F.J. Ahmad and R.K. Khar, Chitosan–sodium Alginate Nanoparticles as Submicroscopic R for Ocular Delivery: Formulation, Optimization and In Vitro Characterisation, *Eur. J. Pharm. Biopharm.*, 2008, **68**(3), p 513–525.
39. N. Mustafa, M.H.I. Ibrahim, R. Asmawi and A.M. Amin, Hydroxyapatite Extracted From Waste Fish Bones and Scales via Calcination Method, *Appl. Mech. Mater.*, 2015, **773–774**, p 287–290.
40. M. Boutinguiza, J. Pou, R. Comesana, F. Lusquinos, A. de Carlos and B. León, Biological Hydroxyapatite Obtained from Fish Bones, *Mater. Sci. Eng. C*, 2012, **32**, p 478–486.
41. A. Pal, S. Paul, A.R. Choudhury, V.K. Balla, M. Das and A. Sinha, Synthesis of Hydroxyapatite from Lates Calcarifer Fish Bone for Biomedical Applications, *Mater. Lett.*, 2017, **203**, p 89–92.
42. S.M. Naga, A.M. Hassan, M. Awaad, A. Killinger, R. Gadow, A. Bernstein and M. Sayed, Forsterite/Nano-Biogenic Hydroxyapatite Composites for Biomedical Applications, *J. Asian Ceram. Soc.*, 2020, **8**(2), p 373–386.
43. DIN EN ISO 17836: Thermal spraying - Determination of the deposition efficiency for thermal spraying <https://dx.doi.org/https://doi.org/10.31030/2723759>
44. A. Wennerberg and T. Albrektsson, Effects of Titanium Surface Topography on Bone Integration: A Systematic Review, *Clin. Oral Implants Res.*, 2009, **20**(4), p 172–184.
45. T. Albrektsson and A. Wennerberg, Oral Implant Surfaces: Part 1—Review Focusing on Topographic and Chemical Properties of

- Different Surfaces and In Vivo Responses to Them, *Int. J. Prosthodont.*, 2004, **17**, p 536–543.
46. J.Y. Park and J.E. Davies, Red blood Cell and Platelet Interactions with Titanium Implant Surfaces, *Clin. Oral Implants Res.*, 2000, **11**(6), p 530–539.
47. N. Iwata, K. Nozaki, N. Horiuchi, K. Yamashita, Y. Tsutsumi, H. Miura and A. Nagai, Effects of Controlled Micro-/Nano Surfaces on Osteoblast Proliferation, *J. Biomed. Mater. Res. Part A*, 2017, **105**, p 2589–2596.
48. M. Franchi, E. Orsini, A. Trire, M. Quaranta, D. Martini, G.G. Piccari, A. Ruggeri and V. Ottani, Osteogenesis and Morphology of the Peri-Implant Bone Facing Dental Implants, *Sci. World J.*, 2004, **4**, p 1083–1095.
49. M. Franchi, B. Bacchelli, G. Giavaresi, V. De Pasquale, D. Martini, M. Fini, R. Giardino and A. Ruggeri, Influence of Different Implant Surfaces on Peri-Implant Osteogenesis: Histomorphometric Analysis in Sheep, *J. Periodontol.*, 2007, **78**(5), p 879–888.
50. R.J. Lazzara, T. Testori, P.M. Trisi, S.S. Porter and R.L. Weinstein, A Human Histologic Analysis of Osseotite and Machined Surfaces Using Implants with 2 Opposing Surfaces, *Int. J. Periodontics Restor. Dent.*, 1999, **19**(2), p 117–129.
51. G. Brunello, H. Elsayed and L. Biasetto, Bioactive Glass and Silicate-Based Ceramic Coatings on Metallic Implants: Open Challenge or Outdated Topic?, *Materials*, 2019, **12**(18), p 2929.
52. P.N. Chavan, M.M. Bahir, R.U. Mene, M.P. Mahabole and R.S. Khairnar, Study of Nanobiomaterial Hydroxyapatite in Simulated Body Fluid: Formation and Growth of Apatite, *Mater. Sci. Eng. B*, 2010, **168**(1–3), p 224–230.
53. J. Lu, M. Descamps, J. Dejoui, G. Koubi, P. Hardouin, J. Lemaitre and J.P. Proust, The Biodegradation Mechanism of Calcium Phosphate Biomaterials in Bone, *J. Biomed. Mater. Res.*, 2002, **63**(4), p 408–412.
54. H. Suito, Y. Iwawaki, T. Goto, Y. Tomotake and T. Ichikawa, Oral Factors Affecting Titanium Elution and Corrosion: An In Vitro Study Using Simulated Body Fluid, *PLoS ONE*, 2013, **8**(6), p e66052.
55. R.K. Singh, S. Awasthi, A. Dhayalan, J.M.F. Ferreira and S. Kannan, Deposition, Structure, Physical and In Vitro Characteristics of Ag-Doped β - $\text{Ca}_3(\text{PO}_4)_2$ /Chitosan Hybrid Composite Coatings on Titanium Metal, *Mater. Sci. Eng. C Mater. Biol. Appl.*, 2016, **62**, p 692–701.
56. L. Benea, E. Danaïla and P. Ponthiaux, Effect of Titania Anodic Formation and Hydroxyapatite Electrodeposition on Electrochemical Behavior of Ti–6Al–4V Alloy Under Fretting Conditions for Biomedical Applications, *Corros. Sci.*, 2015, **91**, p 262–271.
57. E. Dănăilă, L. Benea, The Effect of Surface Roughness on Corrosion Behavior of Ti-6Al-4V Alloy in Saliva Solution. In: *2015 E-Health and Bioengineering Conference (EHB)*, 2015, p 1–4, <https://doi.org/10.1109/EHB.2015.7391518>
58. N. Dumelie, D. Richard, D. Laurent- Maquin and G. Balossier, In Vitro Precipitation of Electrodeposited Calcium-Deficient Hydroxyapatite Coatings on Ti6Al4V Substrate, *Mater. Character.*, 2008, **59**, p 129–133.
59. S.V. Dorozhkin, A Review on the Dissolution Models of Calcium Apatites, *Prog. Cryst. Growth Character. Mater.*, 2002, **44**, p 45–61.
60. M. Sayed, R.A. Gado, S.M. Naga, P. Colombo and H. Elsayed, Influence of the Thermal Treatment on the Characteristics of Porous Geopolymers as Potential Biomaterials, *Mater. Sci. Eng. C*, 2020, **116**, p 111171.

Publisher's Note Springer Nature remains neutral with regard to jurisdictional claims in published maps and institutional affiliations.